Modeling Temperature Dependence of Loads: An Additive Decomposition Approach

Anonymous Author(s)

ABSTRACT

In this paper, we address the increasing need to better understand the relationship between electricity consumption and temperature, especially in the context of rising temperatures and extreme weather events due to climate change. Traditional approaches to electrical load modeling predominantly aim at achieving the best forecasting accuracy, while the task of obtaining a realistic model of temperature dependence is often overlooked. To address these issues, we propose a model that decomposes electrical load into temperature-dependent and time-dependent parts, with the temperature-dependent part being explicitly designed to provide additional insights and incorporate real-world constraints that are not typically present in existing models.

We develop our model using data from 2020 to 2023 provided by Clark Public Utilities, including load measurements for 40 substations and anonymized metadata for the buildings they serve. We supplement this dataset with US census data and NOAA weather data. We demonstrate that our model is capable of fitting observational data well and highlight its usefulness in several practical applications, including long-term forecasting, analyzing the effects of heatwaves on cooling capacity, correlating temperature-dependent load with socioeconomic factors, and estimating the effects of demand response and direct load control.

KEYWORDS

Energy Modeling

ACM Reference Format:

Anonymous Author(s). 2024. Modeling Temperature Dependence of Loads: An Additive Decomposition Approach. In *Proceedings of Make sure to enter the correct conference title from your rights confirmation emai (Conference acronym ACM E-Energy)*. ACM, New York, NY, USA, 10 pages. https://doi.org/XXXXXXX.XXXXXXX

1 INTRODUCTION

Planning and adapting to the impact of climate change is becoming increasingly important for utilities in the US and around the world [15]. Utility planning and operations typically rely on historical and current trends. But as reported by the National Oceanic and Atmospheric Administration (NOAA), the last 10 years in the US (2014 to 2023) are the warmest in recorded history (dating back to 1879) [21], we need to be much more careful in using historical data to make future decisions. In this paper, we provide a data-driven method to understand the impact of climate change on the electric load. In particular, we provide a simple and interpretable method to model the temperature dependency of load.

Since a significant fraction of electric power is used for heating and cooling [37], electricity consumption is strongly influenced by temperature. Across the United States, heating makes up about 14% of all electricity usage, while 16% of electricity is used for cooling [31]. To make decisions, it is useful to have a quantitative characterization of the temperature dependence of loads. A common question that utilities seek to answer when planning for climate change is: suppose the temperature changes by x degrees, how much would load change? A straightforward approach would be to utilize a load forecasting algorithm and vary the input temperature to see the changes in the predicted load [19]. This method, however, often does not accurately reflect the dependence of load in temperature [30].

While temperature is one of the key inputs to load forecasting algorithms, the objective of most forecasting algorithms is to minimize some error metric [16]. State-of-the-art algorithms tend to utilize a litany of features that interact with each other (e.g., temperature and autoregressive features) and advanced machine learning techniques, making isolation of the impact of any one feature difficult [18]. There has been work that make more explicit use of temperature in load forecasting [30], but they are often used to scale or normalize the entire forecast.

Another phenomenon that requires an explicit model of load dependence on temperature is the impact of extreme temperatures on customer behavior. In the summer of 2021, the Pacific Northwest and West regions of the United States experienced an unprecedented heatwave, with temperature reaching over 45 °C (113 °F) [6, 20].[1] Anecdotal evidence suggested that customers in the region installed significantly more cooling to prepare for future heatwaves, but quantifying or even verifying this increase in cooling has been nontrivial, with somewhat conflicting analyses appearing in the literature [5, 10, 34]. Given that more extreme heat is likely in the region, gaining a clearer picture of customers' behavior and load changes responding to temperature is one of the most important problems for electric utilities.

In this paper, we detail a simple approach to modeling temperature-dependent energy consumption. In particular, we disaggregate substation-level load into heating, cooling, and time-dependent (which we call baseline) components using a non-negative least squares model with basis functions for heating and cooling that encode real-world constraints. The resulting model is simple, interpretable, and useful in answering important problems in planning. Using real-world data from a part of Washington State, we consider three applications. First, we show how to use it to study the change

[1] As a comparison, the average daily high for this region during the summer is 25 °C (77 °F) [27].

Conference acronym ACM E-Energy, 2024, Singapore

ACM ISBN 978-1-4503-XXXX-X/18/06
https://doi.org/XXXXXXX.XXXXXXX

in load for different realizations of possible future scenarios. Notably, it turns out that load depends nonlinearly on temperature, and we quantify the impact of some demand response programs. Second, we show how to use census data to understand the correlation between income and temperature dependence of load, providing suggestions to policymakers about possible incentives to alleviate energy poverty. Third, we quantify the change in the cooling load because of the 2021 summer heatwave, showing how users might adapt to a changing climate.

For existing models in the literature, the one in [22] is probably the closest to ours. It also considers a decomposition of load into several components, but these components are learned functions (parameterized by neural networks). This model does not separate heating and cooling, and the contribution of the temperature-driven component can be negative, making interpretations of temperature dependence difficult. The model we use in this paper is at a much higher level than some disaggregation methods that study the temperature dependence of appliances [4, 25]. One reason is that the available data to us is at the substation level. Another reason is that disaggregated models at the appliance level can be too flexible, having multiple options that fit the data. This can lead to overfitting, making generalization to unseen scenarios hard to interpret.

The rest of the paper is organized as follows: Section 2 describes the dataset we use in this paper; Section 3 derives the temperature-dependent load model; Section 4 shows how our model can be used to generate future loads under various temperature profiles, understand the impact of changing thermostat settings, and socioeconomic correlations; and Section 5 characterizes the impact on cooling/heating capacity of discrete extreme weather events.

2 DATASET

Figure 1: Map of Clark County [13], Washington [33]. The county includes a medium-sized city (Vancouver, WA) as well as surrounding rural areas.

In this section, we describe the dataset we used in this paper. This dataset is potentially of independent interest and is publicly available.[2]

2.1 Load Data

The load data we work with in this paper are at the distribution substation level. These substations connect the higher voltage transmission grid to the lower voltage distribution grid, serving as the point of common coupling for downstream customers. They are typically metered at a higher resolution, and more reliably, than individual households.

Our data comes from Clark Public Utility (Clark PUD), which is the local utility for Clark County in the state of Washington (see Fig. 1. The dataset spans January 2021 to January 2023 and includes hourly load measurements at 40 substations as well as anonymized metadata for the buildings they serve. The smallest substation in our dataset serves 2615 buildings and has an average load of 19.6 kW, while the largest serves 22634 buildings and has an average load of 104.5 kW.

2.2 Building Data

In addition to the aggregate load data at each of the substations, we also use building information corresponding to each of the substations. This information contains the location (zip code), types of property (residential or commercial), square footage, built year, and other information about each building. For a more detailed description, please see Appendix 7.3.

An important feature to note is that the number of buildings in the Clark PUD service area has remained roughly constant (within 1.5% year-over-year) over the time period covered by the data. This fact gives us confidence that the changes in load temperature dependence is not simply due to new construction activities.

2.3 Weather Data

We incorporate weather data from NOAA's Local Climatological Dataset[26] for the Clark County region. The meteorological data from NOAA weather stations contains several categories, from air temperature to cloud cover to precipitation. In this paper, since the main goal of this paper is to model the temperature dependence of load, we mainly use temperature information.

2.4 Other Existing Datasets

There are several other load datasets that have been developed, but they all have some drawbacks that can be complemented by the data we use in this paper. For example, a commonly used dataset is the household electricity consumption data from Pecan Street Dataport [29], which includes the metered data for several hundred customers in a particular area. This dataset has been used in load disaggregation [8] and demand response [36] studies. But because it is a snapshot of a small set of customers, it is difficult to draw conclusions to "what if"-type of questions in planning, in particular, would more users install cooling as temperature increases?

Studies about larger sets of customers have typically been conducted as surveys. For example, the Residential Energy Consumption Survey (RECS) [32] provides estimates of end-use residential energy consumption in the United States. The RECS study uses a calibration technique to align energy models with observed billing data. The survey is conducted every 5 years and provides a snapshot of state-level energy consumption for common household end-uses including AC, refrigerators, space heating, water heating, etc.

While the RECS analysis provides good estimates of annual end-use energy consumption at the state level, planning and analysis tasks may require us to understand energy consumption at finer-grained spatial and temporal resolutions. However, obtaining and

[2]To aid the double-blind review process, a link is not provided at this time. A link will be added once anonymity is no longer required.

disseminating individual household-level data for a large number of customers has clear cost and privacy barriers. Recent efforts such as NREL's EULP [35] aim to address these limitations. The EULP dataset is a synthetic dataset of physics-based building models that have been calibrated to match the RECS estimates.

While this synthetic approach leads to better temporal and spatial resolution, the relationship between temperature and load remains largely obscured and not explicitly understood. Namely, the ELUP is constructed assuming that the environment does not drastically change, thus providing a relatively static view of the load profiles. In regions that are experiencing climate change, especially where customers' behaviors are changing as a result, there is no easy way to modify the EULP load profiles to reflect these changes. Moreover, tuning synthetic models is not easy. Because they have so many parameters, it is easy to overfit and obtain models that fit well, but are not reflective of the true load. Therefore, the fitting process in models like EULP does not minimize the least square error,[3], and some care is taken to calibrate the models to be consistent with a wide range of scenarios. This makes the model more robust, but less accurate, hence less useful for understanding the difference in load behavior under different scenarios.

We believe the substation-level dataset used in this paper strikes a good balance in data resolution and modeling assumptions. It has enough spatial and temporal resolution to provide data-driven answers to questions about the temperature dependence of load, without the need to disaggregate the load to the appliance scale.

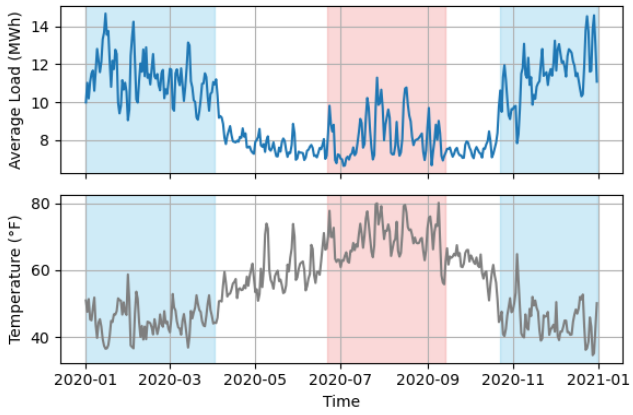

Figure 2: The top panel shows the daily average load for a substation and the bottom panel shows the daily average temperature. The temperature dependence of the load is readily apparent. During the winter (shaded blue) the load increases due to increased heating. Similarly, during the summer (shaded red), the load increases due to increased cooling. The majority of the annual load is due to heating which is expected for a location in the Pacific Northwest.

3 TEMPERATURE DEPENDENT LOAD MODEL

Electrical load consumption depends on a plethora of features, both environmental (e.g., temperature) and behavioral (e.g., holiday vs workday). Most load forecasting algorithms consider all of these features to optimize their fitting performance [3, 16]. The challenge with considering all of these features is that the model includes complicated interactions, and is not easy to interpret or apply in other contexts [17].

In this section, we focus on two main features, temperature and time of the day, that explain most of the electric load. To facilitate explainability, we decompose the load into two components: the temperature-dependent part and the time-dependent part. Later we will show that this simple model performs well, achieving an R^2 of 0.862, explaining 86.2% of the variability in the data.

Decomposing load into additive components is certainly not new. In particular, linear models have been widely used in practice, especially when interpretability is important [1, 2, 24]. However, directly using a linear function of temperature may not be flexible enough. The temperature-dependency of the load is predominantly heating at low temperatures and cooling at high temperatures, which is quite nonlinear. Polynomial basis functions have been used to fit the nonlinearities in the data [11, 12]. However, the predictions given by a polynomial function can be negative or greater than the total installed capacity which is unrealistic. More recently, neural networks have been used to improve the fitting performance, but they still tend to exhibit unrealistic behaviors such as negative load, especially for data points that are outside of the training range [22].

To address these challenges, we first decompose the temperature dependency of load into two distinct functions: cooling and heating. Then we search over functions that have the three following properties:

(1) Nonnegative: The functions should take on nonnegative values.
(2) Monotonic: The cooling function is an increasing function of temperature, and the heating function is a decreasing function of temperature.
(3) Bounded: Cooling and heating functions are upper bounded by some finite values.

The first and second conditions are intuitive. The first one requires that the contribution of heating or cooling should always be positive (or zero), and the second says that load increases as the temperatures get more extreme. The third condition is more subtle and typically not found in existing models. It represents the fact that the heating and cooling have finite capacity, and once all of the capacity is used, changes in temperature have no long-term impact on the load. This condition is also difficult to capture using polynomial basis and generic neural networks [11], leading to the need to explicitly design the functions.

We enforce these properties using the following heating and cooling functions

$$\text{cooling}(T) = \theta_c \, f_c\,(T) \quad \text{and} \quad \text{heating}(T) = \theta_h \, f_h\,(-T)\,,$$

where θ_c and θ_h can be interpreted as the cooling and heating capacity of the region, respectively. Consequently, we can normalize f_c and f_h to have a maximum of 1.

Because the functions f_c and f_h are nonnegative, monotonic, and with maximum values of 1, they can be naturally interpreted as cumulative distribution functions (CDFs). The output of f_c and f_h is interpreted as the fraction of the total capacity that is in use at

[3] Or other commonly used error metrics

temperature T. In Section 3.1, we show that the choice of f_c and f_h has strong consequences on the model's ability to extrapolate outside of the observed temperature range. In this paper, we use the uniform CDf for f_c and f_h. This choice is based on two reasons: first, the uniform CDF provides a conservative extrapolation beyond the observed temperature range; second, we find that it demonstrates a good fit with the data. We denote the parameters of the uniform CDF—the minimum and maximum value of the support—as $\underline{\tau_c}$ and $\overline{\tau_c}$ for cooling, and $\underline{\tau_h}$ and $\overline{\tau_h}$ for heating. The CDF parameters as well as θ_c and θ_h, are learned from data. It turns out that the particular distributions that we use have a support of [57.5 °F, 107 °F] for cooling and [7 °F, 73.6 °F] for heating and are shown in the top panel of Figure 3. We discuss how we obtain the CDF parameters in Section 3.1.

The load is also heavily influenced by the time of the day and the day of the week. We model the baseline load with a lookup table for the time-dependent energy consumption at each hour of the week, see the bottom panel of Figure 3. One way to write mathematically is to one-hot encode the hour of the week and learn the following linear function

$$\text{baseline}(t) = \sum_{i=1}^{168} \theta_i \mathbf{1}_{\{i=\text{mod}(t-1,168)+1\}} = \theta_t^T f_t(t). \tag{1}$$

where $\theta_t = [\theta_1\ \theta_2\ \cdots\ \theta_{168}]^T$ and $f_t(t)$ is a vector containing all zeros except in the $i = \text{mod}(t-1, 168) + 1$ position where it is 1.

Ultimately, we model a substation's net load with the following additive decomposition

$$\hat{y} = \text{baseline}(t) + \text{heating}(T) + \text{cooling}(T) \tag{2}$$

$$= \theta_t^T f_t(t) + \theta_h f_h(-T) + \theta_c f_c(T) \tag{3}$$

where

- t is time, T is temperature
- $\theta_t^T f_t(t)$ is the time-dependent load
- f_c is the cooling load as a fraction of the cooling capacity θ_c
- f_h is the heating load as a fraction of the heating capacity θ_h.

3.1 Model Fitting

To obtain the parameters of the model, we solve the following optimization problem

$$\begin{aligned} \text{minimize} \quad & \|y - \hat{y}\|_2^2 \\ \text{subject to} \quad & \hat{y} = f_t(t) + \theta_h f_h(-T) + \theta_c f_c(T) \\ & \theta_c \geq 0;\ \theta_h \geq 0;\ \theta_i \geq 0\ \forall\ i = 1, 2, \ldots, 168. \end{aligned} \tag{4}$$

This is a non-convex optimization problem since f_c and f_h are non-convex in their parameters. However, if the parameters of f_c and f_h are fixed, then (4) is a non-negative least squares problem that can be solved with standard machine learning libraries such as Scikit-Learn. There are only four CDF parameters so the overall problem easily be solved using an iterative procedure. We chose to use the evolutionary algorithm known as CMA-ES [14] as the optimizer. Let $\theta = \{\theta_t, \theta_h, \theta_c\}$ and $\tau = \{\underline{\tau_c}, \overline{\tau_c}, \underline{\tau_h}, \overline{\tau_h}\}$. Our overall model fitting procedure is as follows:

1) Randomly initialize τ, with the constraints that $\overline{\tau_c} > \underline{\tau_c}$ and $\overline{\tau_h} > \underline{\tau_h}$.
2) Obtain θ by solving (4) with the current values of τ.
3) Pass τ and the objective value to the optimizer to generate new candidates for τ.
4) Repeat steps 2) and 3) until convergence.
5) Return θ and τ.

Figure 3 shows the learned components of the model overlayed on the residuals.

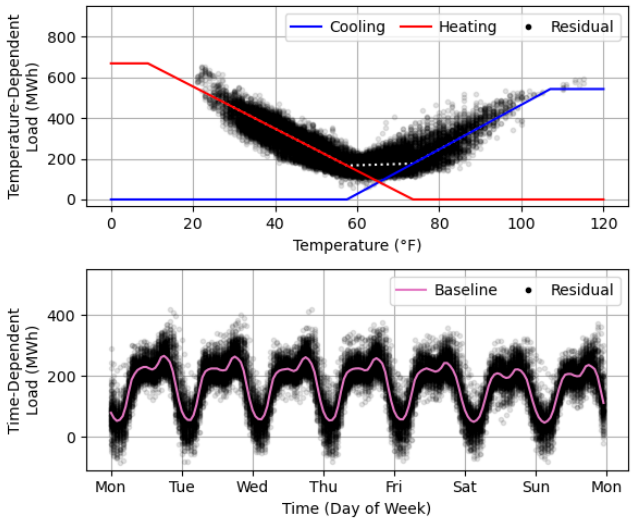

Figure 3: The first panel shows the heating and cooling loads overlayed on the temperature-dependent residual, $y - f_t(t)$). The second panel shows the time-dependent load and time-dependent residual, $y - f_c(T) - f_h(T)$.

3.2 Model Comparison

Model	MAPE	MAE (MWh)	RMSE (MWh)	R^2
Polynomial-1	14.29%	57.53	75.141	0.4904
Polynomial-2	8.33%	33.14	41.769	0.8425
Polynomial-3	8.22%	32.51	41.419	0.8451
Polynomial-4	7.87%	30.87	39.569	0.8587
Polynomial-5	7.87%	30.84	39.528	0.8589
Polynomial-6	7.82%	30.51	39.126	0.8618
Additive NN	7.78%	30.38	38.812	0.8653
FCNN	6.05%	24.01	31.734	0.9108
Ours	7.77%	30.39	39.101	0.8620

Table 1: Comparison of model results. The linear model (Polynomial-1) cannot capture the nonlinear temperature dependence and hence has high errors. The polynomial models of higher degree (Polynomial-2 - Polynomial-6) fit the data better but are outperformed by our model. Our model fits the data similar to the additive neural network (Additive NN). The full-connected neural network (FCNN) provides a reference for the best possible fit to data using only temperature and time as input.

As noted in Section 3, the choice of heating and cooling functions has a large effect on how the model extrapolates outside of the observed temperature range. We also compare our model to a Fully Connected Neural Network (FCNN) which uses time and temperature as input, and an Additive Neural Network (Additive NN), which consists of the sum of two fully connected subnetworks—one using temperature as its only input, and the other using time as its only input. The FCNN serves as the baseline since it should have the best fitting performance by allowing interactions between time and temperature. The Additive NN should be the optimal additive model that can be derived from time and temperature because the functional forms are not constrained. Each of the fully connected networks has two hidden layers each with 100 hidden units, and a skip connection. We train the neural networks using the AdamW optimizer.

In Table 1, we compare the errors made by these models. We find that our additive decomposition gets a smaller root mean squared error (RMSE) when compared to the polynomial models and is on par with the Additive NN. The FCNN has the smallest RMSE, but its improvement over our model with respect to the mean absolute percent error is only about 1.8%.

In Appendix 7.1, we show that polynomial models are not suited for our applications. Specifically, they tend to diverge when the temperature is at the extremes, but these are precisely the scenarios of interest to us.

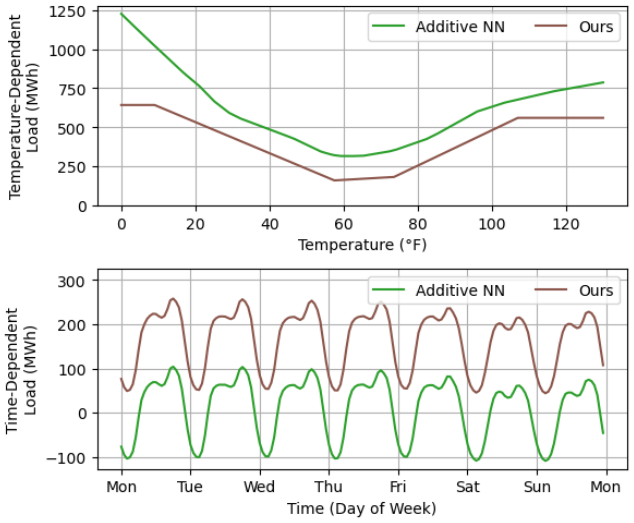

Figure 4: The first panel shows the additive neural network's temperature-dependent predictions and the second panel shows its time-dependent predictions. For comparison, we also show our model's temperature-dependent and time-dependent predictions.

Figure 4 shows the predictions made by the Additive FCNN. We see that the shape of predictions of the Additive NN and our model tend to agree with each other with an exception being at the temperature extremes. However, the Additive NN predicts that the time-dependent load can be negative. While it is true that we could shift the Additive NN's predictions so that they are non-negative, the amount that we shift them is ambiguous. Furthermore, the temperature-dependent predictions of the Additive NN grow unboundedly. We believe the uniform CDF model that we chose is more reasonable at temperature extremes than the learned neural network model. In the city of Vancouver, WA, the mean daily minimum temperature in the winter is about 35 °F (1.7 °C) [27]. Suppose the temperature reaches 20 °F (-6.7 °C), we expect that most of the heating capacity would be on, and there should not be a large increase in heating load if the temperature drops further. This is reflected by our model, but Additive FCNN is too aggressive at the temperature extremes.

Figure 5 shows the predictions made by the FCNN for two training runs with different random seeds. Despite having very similar training errors, the models' predictions can vary significantly from each other. Thus, the FCNN will not provide consistent results in the applications that we discuss below.

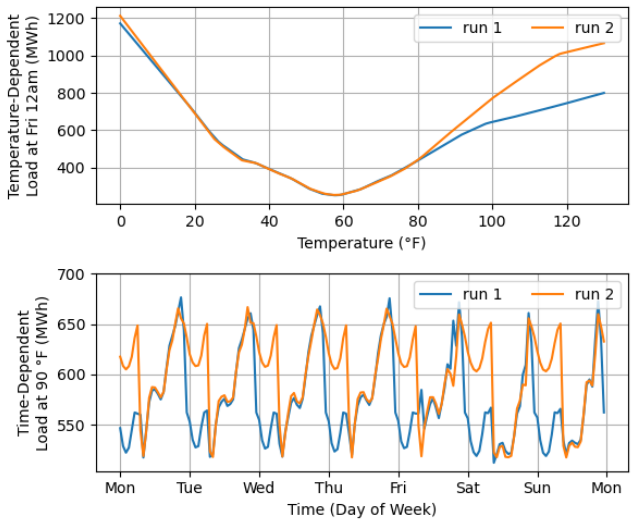

Figure 5: The first panel shows how the FCNN's predictions vary with temperature at a fixed point in time, specifically Friday 12:00 AM. The second panel shows how the FCNN's predictions vary with time at a fixed temperature value of 90 °F.

4 APPLICATIONS

4.1 Future Load Modeling

Predicting future energy consumption is an important component of transmission and distribution planning. This task is made more difficult by the effects of climate change which can change local weather patterns and hence energy consumption patterns. To estimate the effects of future weather conditions on energy consumption we set up a simple experiment where we add Gaussian noise with mean 1 and a standard deviation of 1 to the observed temperatures from January 2021 to September 2022. More sophisticated temperature predictions can easily be used as well.

This example highlights the effects of increased average temperature and increased temperature variability. We use the predicted load from January 2021 to September 2022 as a reference and refer to the change as the difference between the new and reference aggregate load (a positive value means the load corresponding to the new temperature is larger than the reference load). Figure 6 shows the average and maximum change in load aggregated each month[4]. During the summer months, the higher average temperatures lead to a non-negligible increase in the average and maximum cooling loads. However, during the winter months, the average and maximum cooling barely increase. It's interesting to note that the total energy usage decreases because of the increase in mean temperature since the increase in cooling is outweighed by the decrease in heating.

In contrast, the maximum load for heating and cooling increases because of temperature variability. The further divergence between average power and peak power consumption introduces additional challenges in planning, particularly in the types of generation assets that need to be procured and how they should be operated. For a region like the Pacific Northwest of the United States, where cheap and reliable hydropower has largely been tapped out [23], meeting the changes in demand as a consequence of climate change efficiently and sustainably is nontrivial and is an important future direction for us.

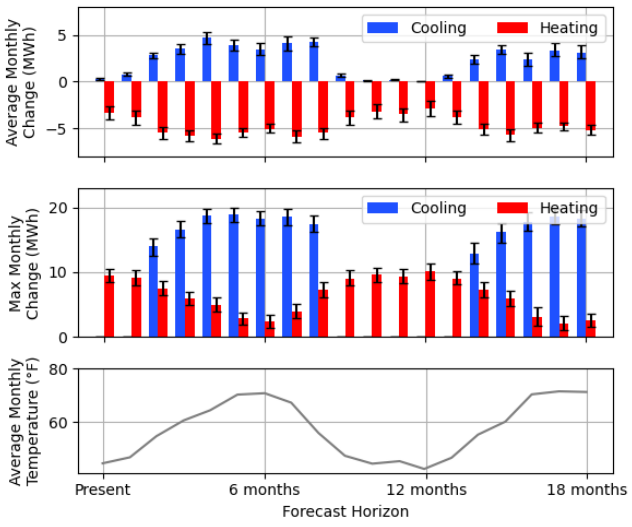

Figure 6: This figure shows the change in load caused by a change in temperature following a Gaussian distribution with a mean and standard deviation of 1 °F. The top panel shows the average hourly change in load, the middle panel shows the maximum hourly change in load, and the bottom panel shows the average temperature after adding Gaussian noise, all values are aggregated by month.

[4]We first calculate the change and then aggregate. Specifically, we are calculating the maximum change which is not necessarily the same as the change in the maximum.

4.2 Effects of Changing Thermostat Settings

In this section, we show how our model can be used to estimate the effects of demand response. As an example, we estimate the effects of cooling loads adjusting their thermostat settings during a heatwave. This is a common type of demand response, where utilities request load adjustments during extreme weather. For simplicity, we assume that the temperature-dependent load is made up entirely of setpoint devices under direct load control. In this case, the cooling CDF $f_c(T)$ represents the fraction of devices that are on at a temperature T. Suppose the utility reduces the setpoint by ΔT, then the new cooling load will be $f_c(T - \Delta T)$. This is in effect the same as shifting the cooling function to the right by ΔT units, see Figure 7. Alternatively, we can assume that the utility asks its users to behave as if it were ΔT degrees cooler. In practice, not all customers would respond to a request to change their setpoints or to reduce power power consumption. In this case, ΔT would scaled by the fraction of users that have responded.

As an example, we consider again the heatwave from June 26 to July 2, 2021. In this case, the temperature exceeded 107 °F which is when our model predicts that the cooling load saturates. Thus, if the current temperature is 110 °F, then reducing the setpoints by $\Delta T < 3$ °F will result in no change in the load. However, if $\Delta T = 4$ °F, then we would expect the load to reduce by roughly 11.32 MWh. This suggests that the impact of changing thermostat setpoints is nonlinear, especially during extreme events. This conclusion is different than other reported studies that report the largest marginal gain at small setpoint adjustments [9].

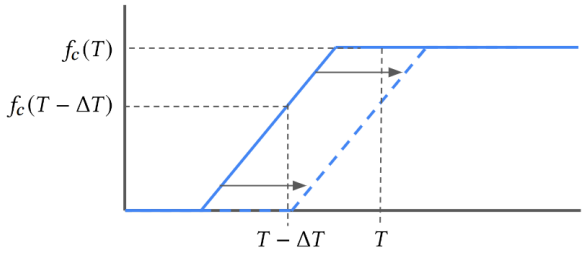

Figure 7: This figure shows the effects of direct load control on cooling. The result is effectively the same as everyone behaving as if it were ΔT degrees cooler.

4.3 Socioeconomic Correlations

In this section, we analyze how income levels in different areas of Clark County correlate with heating and cooling demands. It is plausible that lower-income individuals use more heating and cooling due to having older, less efficient appliances and less insulation. It is also possible that lower-income individuals are more frugal and thus use less heating and cooling. In this section, we show how insights from our model can be used to address energy equity issues, such as identifying areas where lower-income households may face higher energy burdens during extreme temperatures. In

particular, we analyze the relationship between median income[5] and the estimated cooling and heating loads per person[6]. Figure 8 shows that there is a small positive correlation between income and both heating and cooling loads. Thus, this analysis suggests that lower-income communities use less heating and cooling. For more details, please see Table 3 in Appendix 7.4.

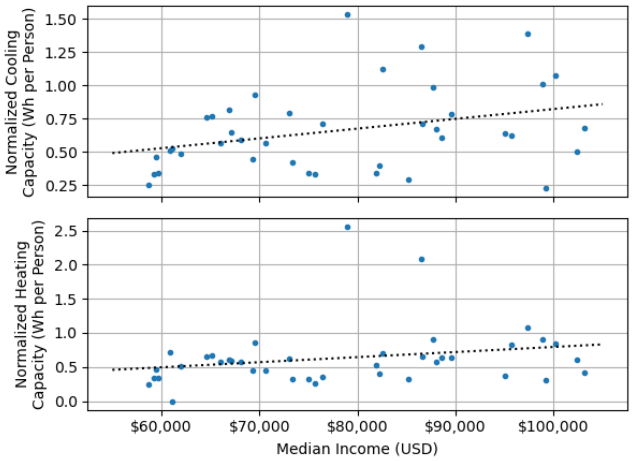

Figure 8: The top panel shows the cooling capacity per person at each substation vs the median income of that substation. The bottom panel shows the same for heating. The dotted lines show the best linear fit to the data.

5 EFFECTS OF HEAT WAVES ON COOLING CAPACITY

Climate change is leading to more extreme temperature variations, especially in locations that are historically mild; for example, heatwaves in the Pacific Northwest and below-freezing temperatures in Texas [28]. An important factor in planning and policy decisions is to understand whether extreme weather events can lead not only to an increase in the utilization of heating and cooling but also to an increase in their installed capacities. Furthermore, quantifying the potential increase in capacity is of interest.

In this section, we show how our model can be used to determine if the heating and cooling capacities increase after extreme events. Without loss of generality, we focus on heatwaves and the changes in cooling capacity. We extend our model in Eq. (3) to include an additional term representing the change in cooling capacity due to the heat wave

$$y = \theta_t^T f_t(t) + \theta_h f_h(-T) + \theta_c f_c(T) + \Delta \, \mathbf{1}_{\{t \geq t_{\text{event}}\}} f_c(T) + \varepsilon$$

where t_{event} is the time of the heat wave, Δ is the change in cooling capacity due to the heat wave, and ε is random noise. We'd like to determine whether $\Delta > 0$ and whether this occurred by chance or whether the value that we estimate is statistically significant. To do this, we show that the estimate for Δ is large compared to its variance and hence is unlikely to have occurred by chance.

We define the following variables corresponding to the i^{th} observation

$$X_{1,i} = \left[\; f_t(t_i)^T \;\middle|\; f_h(-T_i) \;\middle|\; f_c(T_i) \; \right],$$
$$X_{2,i} = \mathbf{1}_{\{t_i \geq t_{\text{event}}\}} f_c(T_i),$$

for all $i = 1, \ldots, N$. Next, we stack the data into the following matrices

$$X_1 = \begin{bmatrix} X_{1,1} \\ X_{1,2} \\ \vdots \\ X_{1,N} \end{bmatrix}, \quad X_2 = \begin{bmatrix} X_{2,1} \\ X_{2,2} \\ \vdots \\ X_{2,N} \end{bmatrix}, \quad Y = \begin{bmatrix} y_1 \\ y_2 \\ \vdots \\ y_N \end{bmatrix}, \quad \varepsilon = \begin{bmatrix} \varepsilon_1 \\ \varepsilon_2 \\ \vdots \\ \varepsilon_N \end{bmatrix},$$

and form the following quantities

$$X = \left[\; X_1 \;\middle|\; X_2 \; \right] \quad \text{and} \quad \beta = \begin{bmatrix} \theta_t \\ \theta_h \\ \theta_c \\ \Delta \end{bmatrix}.$$

We can now write our problem in the standard linear regression notation

$$Y = X\beta + \varepsilon.$$

We assume $\varepsilon_i \sim \mathcal{N}(0, \sigma_e^2)$ are *i.i.d.* and so the least squares estimator is

$$\hat{\beta} = (X^T X)^{-1} X^T Y \sim \mathcal{N}\left(\beta, \sigma_e^2 (X^T X)^{-1}\right).$$

We are interested in the covariance of $\hat{\beta}$ and in particular the value corresponding to Δ. In Appendix 7.2, we show that

$$\text{Var}(\hat{\Delta}) = \frac{\sigma_e^2}{X_2^T X_2 - X_2^T X_1 (X_1^T X_1)^{-1} X_1^T X_2}.$$

We do not necessarily know σ_e^2, but we can estimate it, for example from the residuals of our model using

$$\sigma_e^2 \approx \frac{1}{N} \sum_{i=1}^{N} (y_i - \hat{y}_i)^2.$$

Given $\text{Var}(\hat{\Delta})$, we can now calculate confidence intervals for $\hat{\Delta}$. If the estimated value of Δ is large relative to θ_c, then we can infer that the change in cooling capacity did not happen by chance.

We apply our method to the heat wave that affected Washington from June 26 to July 2, 2021. We summarize our findings in Table 2. We find that the increase in cooling capacity Δ is roughly $9\% - 11\%$ relative to the estimated cooling capacity θ_c. This is also shown in Figure 9 where there is a non-negligible improvement in the model fit when we include the adjustment in cooling after the heat wave.

Parameter	Estimated Value	95% Confidence Interval
θ_c	527.8	[522.0, 533.5]
Δ	53.8	[48.6, 59.0]

Table 2: Estimated values for the heat wave adjusted model.

[5]Some substations serve more than one ZIP code. To calculate the median income, we take a weighted average of all the ZIP code's median income with the weight corresponding to the fraction of buildings in the ZIP code.
[6]We calculate the cooling and heating per person by normalizing θ_c and θ_h by the census population values

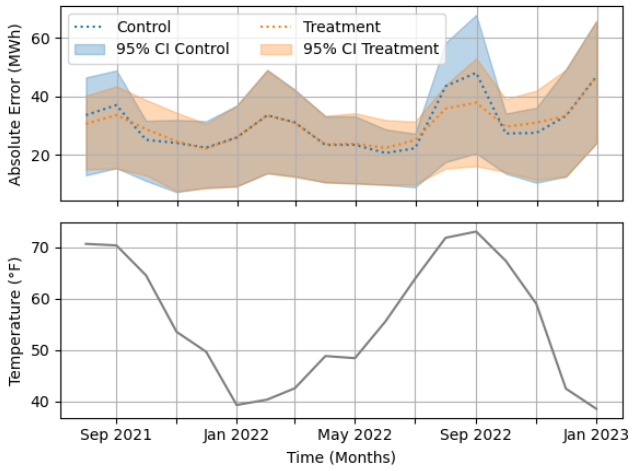

Figure 9: Absolute error calculated each month for the control model where $\Delta = 0$ and the treatment model where $\Delta \neq 0$. The dotted line is the Mean Absolute Error and the shaded regions correspond a the 95% confidence interval.

6 CONCLUSION

In this paper, we investigate the effects of temperature on electrical load. We develop a model that decomposes electrical load into the sum of temperature-dependent and time-dependent parts. Our model is designed to respect the physical limitations of heating and cooling systems, thereby avoiding unrealistic predictions common in polynomial and neural network-based models. We provide a number of applications, from developing long-term electricity demand forecasts to aiding utilities and policymakers in planning for and mitigating the effects of heat waves. Our study contributes a useful tool for electrical load modeling, one that balances accuracy with explainability.

Looking ahead, there are several promising directions for further research. Expanding the model to incorporate additional variables and data sources could enhance its predictive power and applicability to a broader range of problems. Better quantifying the uncertainties associated with the model's predictions could provide value in many downstream applications.

REFERENCES

[1] Nazih Abu-Shikhah and Fawwaz Elkarmi. 2011. Medium-term electric load forecasting using singular value decomposition. *Energy* 36, 7 (2011), 4259–4271.

[2] Hamed Ahmadi and José R Martı. 2015. Load decomposition at smart meters level using eigenloads approach. *IEEE transactions on Power Systems* 30, 6 (2015), 3425–3436.

[3] Hesham K Alfares and Mohammad Nazeeruddin. 2002. Electric load forecasting: literature survey and classification of methods. *International journal of systems science* 33, 1 (2002), 23–34.

[4] Anmar Arif, Zhaoyu Wang, Jianhui Wang, Barry Mather, Hugo Bashualdo, and Dongbo Zhao. 2017. Load modeling—A review. *IEEE Transactions on Smart Grid* 9, 6 (2017), 5986–5999.

[5] Alan Barreca, R Jisung Park, and Paul Stainier. 2022. High temperatures and electricity disconnections for low-income homes in California. *Nature Energy* 7, 11 (2022), 1052–1064.

[6] Samuel Bartusek, Kai Kornhuber, and Mingfang Ting. 2022. 2021 North American heatwave amplified by climate change-driven nonlinear interactions. *Nature Climate Change* 12, 12 (2022), 1143–1150.

[7] Dennis S. Bernstein. 2011. *Matrix Mathematics: Theory, Facts, and Formulas* (second ed.). Princeton University Press.

[8] Hong-An Cao, Tri Kurniawan Wijaya, Karl Aberer, and Nuno Nunes. 2015. A collaborative framework for annotating energy datasets. In *2015 IEEE International Conference on Big Data (Big Data)*. IEEE, 2716–2725.

[9] David P Chassin, Jakob Stoustrup, Panajotis Agathoklis, and Nedjib Djilali. 2015. A new thermostat for real-time price demand response: Cost, comfort and energy impacts of discrete-time control without deadband. *Applied Energy* 155 (2015), 816–825.

[10] Nicole A Errett, Cat Hartwell, Juliette M Randazza, Amruta Nori-Sarma, Kate R Weinberger, Keith R Spangler, Yuantong Sun, Quinn H Adams, Gregory A Wellenius, and Jeremy J Hess. 2023. Survey of extreme heat public health preparedness plans and response activities in the most populous jurisdictions in the United States. *BMC public health* 23, 1 (2023), 1–11.

[11] Shu Fan and Rob J Hyndman. 2012. Forecasting electricity demand in Australian National Electricity Market. In *2012 IEEE Power and Energy Society General Meeting*. 1–4. https://doi.org/10.1109/PESGM.2012.6345304

[12] Anthony Faris, Dmitry Kosterev, Joseph H. Eto, and Dave Chassin. 2020. Load Composition Analysis in Support of the NERC Load Modeling Task Force. 2019-2020 Field Test of the Composite Load Model. https://www.osti.gov/biblio/1644285.

[13] gis.clark.wa.gov. [n. d.]. Maps Online Clark County Washington. https://gis.clark.wa.gov/mapsonline/. Accessed: 2024-01-10.

[14] Nikolaus Hansen, Youhei Akimoto, and Petr Baudis. 2019. CMA-ES/pycma on Github. Zenodo, DOI:10.5281/zenodo.2559634. https://doi.org/10.5281/zenodo.2559634

[15] Juliet S Homer, Alan C Cooke, Kamila Kazimierczuk, Rebecca Tapio, Julie Peacock, and Abigail King. 2023. *Emerging Best Practices for Electric Utility Planning with Climate Variability*. Technical Report. Pacific Northwest National Labs.

[16] Tao Hong and Shu Fan. 2016. Probabilistic electric load forecasting: A tutorial review. *International Journal of Forecasting* 32, 3 (2016), 914–938.

[17] Tao Hong, Min Gui, Mesut E Baran, and H Lee Willis. 2010. Modeling and forecasting hourly electric load by multiple linear regression with interactions. In *Ieee pes general meeting*. IEEE, 1–8.

[18] Tao Hong, Pierre Pinson, Yi Wang, Rafał Weron, Dazhi Yang, and Hamidreza Zareipour. 2020. Energy forecasting: A review and outlook. *IEEE Open Access Journal of Power and Energy* 7 (2020), 376–388.

[19] Maryam Imani. 2021. Electrical load-temperature CNN for residential load forecasting. *Energy* 227 (2021), 120480.

[20] Julie Ingwersen. 2021. Wither away and die: U.S. Pacific Northwest heat wave bakes wheat, fruit crops. *Reuters* (2021).

[21] REBECCA LINDSEY and LUANN DAHLMAN. 2024. Climate Change: Global Temperature. https://www.climate.gov/news-features/understanding-climate/climate-change-global-temperature.

[22] Hengbo Liu, Ziqing Ma, Linxiao Yang, Tian Zhou, Rui Xia, Yi Wang, Qingsong Wen, and Liang Sun. 2023. SaDI: A Self-adaptive Decomposed Interpretable Framework for Electric Load Forecasting under Extreme Events. arXiv:2306.08299 [cs.LG]

[23] Matthew S Markoff and Alison C Cullen. 2008. Impact of climate change on Pacific Northwest hydropower. *Climatic Change* 87, 3-4 (2008), 451–469.

[24] Neethu Mohan, KP Soman, and S Sachin Kumar. 2018. A data-driven strategy for short-term electric load forecasting using dynamic mode decomposition model. *Applied energy* 232 (2018), 229–244.

[25] Mohammed K Muthalib and Chika O Nwankpa. 2016. Physically-based building load model for electric grid operation and planning. *IEEE Transactions on Smart Grid* 8, 1 (2016), 169–177.

[26] National Oceanic and Atmospheric Administration. [n. d.]. Local Climatological Data. https://www.ncei.noaa.gov/access/metadata/landing-page/bin/iso?id=gov.noaa.ncdc:C00128. Accessed: 2023-03-21.

[27] National Oceanic and Atmospheric Administration. 2024. NowData – NOAA Online Weather Data. https://www.weather.gov/wrh/climate?wfo=sew.

[28] National Weather Service. 2021. Valentine's Week Winter Outbreak 2021: Snow, Ice, & Record Cold. https://www.weather.gov/hgx/2021ValentineStorm.

[29] Pecan Street Dataport. 2024. https://dataport.pecanstreet.org.

[30] Kyung-Bin Song, Seong-Kwan Ha, Jung-Wook Park, Dong-Jin Kweon, and Kyu-Ho Kim. 2006. Hybrid load forecasting method with analysis of temperature sensitivities. *IEEE Transactions on Power Systems* 21, 2 (2006), 869–876.

[31] The U.S. Energy Information Administration. 2023. Annual Energy Outlook. https://www.eia.gov/outlooks/aeo/.

[32] U.S. Energy Information Administration. 2020. Residential Energy Consumption Survey (RECS). https://www.eia.gov/consumption/residential/. Accessed: 2024-01-16.

[33] WaterproofPaper.com. [n. d.]. Printable Washington Map Collection. https://www.waterproofpaper.com/printable-maps/washington/printable-washington-county-map.pdf. Accessed: 2024-01-10.

[34] Rachel H White, Sam Anderson, James F Booth, Ginni Braich, Christina Draeger, Cuiyi Fei, Christopher DG Harley, Sarah B Henderson, Matthias Jakob, Carie-Ann Lau, et al. 2023. The unprecedented Pacific Northwest heatwave of June

2021. *Nature Communications* 14, 1 (2023), 727.
[35] Eric Wilson, Andrew Parker, Anthony Fontanini, Elaina Present, Janet Reyna, Rajendra Adhikari, Carlo Bianchi, Christopher CaraDonna, Matthew Dahlhausen, Janghyun Kim, Amy LeBar, Lixi Liu, Marlena Praprost, Philip White, Liang Zhang, Peter DeWitt, Noel Merket, Andrew Speake, Tianzhen Hong, Han Li, Natalie Mims Frick, Zhe Wang, Aileen Blair, Henry Horsey, David Roberts, Kim Trenbath, Oluwatobi Adekanye, Eric Bonnema, Rawad El Kontar, Jonathan Gonzalez, Scott Horowitz, Dalton Jones, Ralph Muehleisen, Siby Platthotam, Matthew Reynolds, Joseph Robertson, Kevin Sayers, and Qu. Li. 2021. End-Use Load Profiles for the U.S. Building Stock. https://data.openei.org/submissions/4520.
[36] Bainan Xia, Hao Ming, Ki-Yeob Lee, Yuanyuan Li, Yuqi Zhou, Shantanu Bansal, Srinivas Shakkottai, and Le Xie. 2017. Energycoupon: A case study on incentive-based demand response in smart grid. In *Proceedings of the Eighth International Conference on Future Energy Systems*. 80–90.
[37] Hai-xiang Zhao and Frédéric Magoulès. 2012. A review on the prediction of building energy consumption. *Renewable and Sustainable Energy Reviews* 16, 6 (2012), 3586–3592.

7 APPENDICES

7.1 Polynomial Model of Temperature Dependence

Figure 10 shows the predictions made by the polynomial models. The time-dependent load of the polynomial models tends to agree with each other; however, the temperature-dependent predictions of the polynomial models disagree with each other at the temperature extremes.

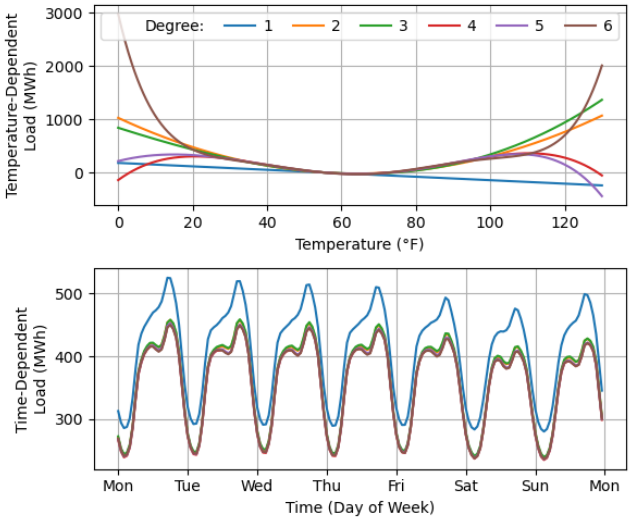

Figure 10: Models with polynomial functions for the temperature-dependent component. Note the disagreement in the temperature-dependent predictions at the temperature extremes where the data is limited. This is a common problem with polynomial models which makes them unreliable at extrapolating to new temperature extremes. Note that the time-dependent load is very similar for all the models.

7.2 Derivations for the Effects of Heat Waves on Cooling Capacity

We are interested in the variance of this estimator or

$$\mathrm{Var}(\hat{\beta}) = \mathbb{E}\left[(\beta - \hat{\beta})(\beta - \hat{\beta})^T\right]. \tag{5}$$

To compute this, observe that

$$\begin{aligned}\hat{\beta} &= (X^TX)^{-1}X^TY = (X^TX)^{-1}X^T(X\beta + \varepsilon)\\ &= \beta + (X^TX)^{-1}X^T\varepsilon\end{aligned}$$

Substituting this into Eq. 5 yields

$$\begin{aligned}\mathrm{Var}(\hat{\beta}) &= \mathbb{E}\left[(\beta - \hat{\beta})(\beta - \hat{\beta})^T\right]\\ &= \mathbb{E}\left[(X^TX)^{-1}X^T\varepsilon\varepsilon^TX(X^TX)^{-1}\right]\\ &= (X^TX)^{-1}X^T\mathbb{E}\left[\varepsilon\varepsilon^T\right]X(X^TX)^{-1}\\ &= (X^TX)^{-1}X^T(\sigma_e^2 I)X(X^TX)^{-1}\\ &= \sigma_e^2(X^TX)^{-1}.\end{aligned}$$

Writing out X^TX in terms of X_1 and X_2 gives

$$X^TX = \begin{bmatrix} X_1^TX_1 & X_1^TX_2 \\ X_2^TX_1 & X_2^TX_2 \end{bmatrix}.$$

The inverse of a 2×2 matrix is given by

$$\begin{bmatrix} A & B \\ C & D \end{bmatrix}^{-1} = \begin{bmatrix} A^{-1} + A^{-1}BS^{-1}CA^{-1} & -A^{-1}BS^{-1} \\ -S^{-1}CA^{-1} & S^{-1} \end{bmatrix},$$

where $S^{-1} = (D - CA^{-1}B)^{-1}$ is the inverse of the Schur complement [7]. We are interested in the bottom right entry of the inverse which corresponds to

$$\begin{aligned}\mathrm{Var}(\hat{\Delta}) &= \sigma_e^2\left(X_2^TX_2 - X_2^TX_1(X_1^TX_1)^{-1}X_1^TX_2\right)^{-1}\\ &= \frac{\sigma_e^2}{X_2^TX_2 - X_2^TX_1(X_1^TX_1)^{-1}X_1^TX_2}.\end{aligned}$$

7.3 Building Metadata

The dataset includes the following variables:

- SubstationID and FeederID: These columns identify the substations and feeders. There are 41 unique substations and 7 feeder IDs in the dataset.
- Zip: Zip codes where the buildings are located.
- PropertyUseClass: Describes the use class of the property, for example, 'residential' or 'commercial'.
- Pt1Desc and Pt2Desc: These columns provide descriptions related to the property.
- BldgSqft: Building square footage, varying widely across the dataset.
- BldgType: Type of building, with 'CONVENTIONAL' being the most common.
- Units: The number of units in the building.
- BldgYrBlt and BldgEffYrBlt: Year the building was built and its effective year built.
- Year: The year when the data was recorded.

7.4 Model Fit Per Substation

The follow table provides more details about the data discussed in Section 4.3.

Substation	Median Income (USD)	Total Population	Cooling Capacity (MWh)	Heating Capacity (MWh)	MAPE	MAE (MWh)	RMSE (MWh)	R^2
STN01	59417	40458	18.72	18.63	9.05%	0.876	1.137	0.809
STN02	66005	39957	22.44	23.18	9.05%	1.075	1.376	0.816
STN03	70601	27811	15.73	12.55	9.19%	0.691	0.935	0.775
STN04	61955	37954	18.55	19.38	10.30%	0.997	1.298	0.758
STN05	94999	37961	24.24	14.35	12.62%	1.283	1.685	0.614
STN06	65134	27440	20.97	18.28	9.74%	1.127	1.441	0.716
STN07	64591	26513	20.05	17.51	12.64%	1.375	1.758	0.559
STN08	59677	37848	12.89	12.94	10.00%	0.716	0.923	0.727
STN09	61074	39484	20.77	0.00	19.90%	1.724	2.539	0.447
STN10	89574	23020	18.07	14.85	8.20%	0.882	1.151	0.749
STN11	97331	24704	34.27	26.52	8.91%	1.531	2.001	0.738
STN12	59263	45920	15.38	15.69	6.67%	0.826	1.061	0.816
STN13	102343	29288	14.69	17.81	11.97%	1.042	1.371	0.677
STN14	98911	19957	20.06	17.92	10.23%	0.931	1.235	0.749
STN16	88068	24124	16.26	13.81	11.81%	0.894	1.170	0.612
STN17	82555	25423	28.47	17.74	11.92%	1.624	2.123	0.556
STN18	86494	8937	11.54	18.56	11.78%	0.964	1.249	0.750
STN19	88615	31810	19.20	20.43	10.32%	1.238	1.565	0.719
STN20	73032	27270	21.64	17.04	7.71%	0.839	1.093	0.815
STN21	86590	34665	24.68	22.91	11.05%	1.304	1.673	0.711
STN22	68050	30842	18.15	17.83	8.25%	0.801	1.048	0.848
STN23	67167	24763	16.02	14.65	10.82%	0.993	1.283	0.611
STN28	75035	58725	19.95	19.00	9.66%	0.967	1.242	0.796
STN29	69275	36355	16.14	16.38	9.13%	0.797	1.050	0.801
STN32	75629	60878	20.18	16.17	9.32%	1.012	1.370	0.680
STN33	103111	29791	20.21	12.27	9.42%	0.816	1.072	0.763
STN35	76405	33048	23.39	11.62	8.45%	1.244	1.562	0.689
STN37	73359	46061	19.41	15.26	8.23%	0.826	1.047	0.803
STN40	100213	28261	30.40	23.99	8.59%	1.389	1.802	0.786
STN41	66858	29462	24.09	18.03	9.90%	1.291	1.704	0.731
STN42	95642	20886	13.05	17.26	15.08%	1.192	1.575	0.517
STN43	60873	14669	7.49	10.48	5.30%	0.739	1.071	0.835
STN44	82263	48400	18.99	19.37	10.43%	0.979	1.262	0.755
STN46	99146	20505	4.60	6.21	13.22%	0.376	0.497	0.625
STN47	87726	28416	28.08	25.56	12.25%	1.687	2.144	0.609
STN48	85162	37215	10.82	12.04	10.66%	0.646	0.846	0.740
Total	78948	2265461	560.24	642.49	7.77%	30.39	39.10	0.862

Table 3: Substation level information and model fitting results.